

DFT study of $\text{La}_2\text{Ce}_2\text{O}_7$: disordered fluorite vs pyrochlore structure

D. E. P. Vanpoucke,¹ P. Bultinck,¹ S. Cottenier,² V. Van Speybroeck,² and I. Van Driessche¹

¹*Dept. Inorganic and Physical Chemistry, Ghent University, Krijgslaan 281 - S3, 9000 Gent, Belgium*

²*Center for Molecular Modeling, Ghent University, Technologiepark 903, 9053 Zwijnaarde, Belgium*

(Dated: September 28, 2018)

The crystal structure of Lanthanum Cerium Oxide ($\text{La}_2\text{Ce}_2\text{O}_7$) is investigated using *ab initio* density functional theory (DFT) calculations. The relative stability of fluorite- and pyrochlore-like structures is studied through comparison of their formation energies. These formation energies show the pyrochlore structure to be favored over the fluorite structure, apparently contradicting the conclusions based on experimental neutron and X-ray diffraction (XRD). By calculating and comparing XRD spectra for a set of differently ordered and random structures, we show that the pyrochlore structure is consistent with diffraction experiments. For these reasons, we suggest the pyrochlore structure as the ground state crystal structure for $\text{La}_2\text{Ce}_2\text{O}_7$.

PACS numbers:

I. INTRODUCTION

Since the pioneering work of Zintl and Croatto,¹ $\text{La}_2\text{Ce}_2\text{O}_7$ has been studied for over half a century. During this time, $\text{La}_2\text{Ce}_2\text{O}_7$ and more generally the $\text{La}_x\text{Ce}_{1-x}\text{O}_{2-x/2}$ compounds have been studied in the context of three-way automotive catalysts,²⁻⁵ as an ionic conductor in solid oxide fuel cells,⁶⁻⁸ and as oxygen sensor. In recent years, it has also become of interest as a new material for thermal barrier coatings.⁹⁻¹¹ It might also be considered as a new buffer layer in combination with perovskite superconductors for the use in coated conductors on Rolling Assisted Biaxially Textured substrates (RABiTS).¹²⁻¹⁴

Although this compound has been known for a long time, its crystal structure remains a point of discussion. The two competing models for its crystal structure are the disordered fluorite and the pyrochlore structures.

Many ternary oxides with the formula $\text{A}_2\text{B}_2\text{O}_7$, with +III ions A and +IV ions B, adopt a pyrochlore structure, making the latter a good candidate for the $\text{La}_2\text{Ce}_2\text{O}_7$ structure. Conversely, in many cases where a pyrochlore crystal structure is observed, the A and B ions are indeed lanthanides and/or transition metals. A pyrochlore structure (space group $Fd\bar{3}m$) can be obtained from a fluorite structure (space group $Fm\bar{3}m$) with one eighth of the oxygen ions missing ($Fd\bar{3}m$ Wickoff 8a site, when placing the origin at a B cation). Each oxygen vacancy is surrounded by four B^{IV} ions (16c sites), while six oxygen ions (48f sites) are each surrounded by two A^{III} and two B^{IV} ions, and the seventh oxygen ion (8b site) is surrounded by four A^{III} ions (16d sites). The pyrochlore structure has a clear short-range order. It turns out to be stable only in a certain range of ionic radius ratios of the two cations. Outside this range, a disordered fluorite structure becomes more stable.¹⁵

This *disordered* fluorite structure for $\text{La}_2\text{Ce}_2\text{O}_7$ is obtained by random replacement of half the Ce cations in the CeO_2 cubic fluorite lattice by La cations. In addition, one eighth of the O anions are removed, also through random selection. This structure has the required stoichiometry

and the crystal structure is a cubic fluorite with each cation site occupied by 0.5 Ce and 0.5 La atoms on average, and each anion site on average occupied by 0.875 O atoms. As a result, no short-range order is present in a disordered fluorite structure, in contrast to the pyrochlore structure, .

The border between the stability regions of the disordered fluorite and the pyrochlore structures has been defined empirically, to reflect the experimental data as well as possible.¹⁶ With the ionic radius ratio for $\text{La}_2\text{Ce}_2\text{O}_7$ located very close to this border, $\text{La}_2\text{Ce}_2\text{O}_7$ itself becomes interesting for investigating the order-disorder transition in pyrochlores. Minervini *et al.* show in their theoretical study of disorder in pyrochlore oxides that $\text{La}_2\text{Ce}_2\text{O}_7$ lies at the boundary of stability for pyrochlore formation. They claim that in this boundary region $\text{La}_2\text{Ce}_2\text{O}_7$ remains a disordered fluorite structure, though the pyrochlore structure appears stable with regard to cation and anion disorder.¹⁶

Furthermore, there is a list of experiments which are in favor of the disordered fluorite structure. In their early neutron diffraction experiments, Brisse and Knop claim $\text{La}_2\text{Ce}_2\text{O}_7$ to have a disordered fluorite structure rather than a pyrochlore one.¹⁵ But also more recent XRD experiments point towards a disordered fluorite structure, due to the lack of pyrochlore-specific peaks in the spectrum.^{17,18} It was also shown that this structure remains stable, even at very high temperatures.^{9,10}

In contrast, recent studies of $\text{La}_x\text{Ce}_{1-x}\text{O}_{2-x/2}$ show a different behavior. XRD experiments by Bae *et al.*⁸ show that the CeO_2 fluorite structure is maintained for La concentrations up to $x = 0.40$ (for $\text{La}_2\text{Ce}_2\text{O}_7$ $x = 0.50$), and only at higher La concentrations the pyrochlore ordering of the cations (La^{III} and Ce^{IV}) appears. These authors also observe that the lattice parameter does not expand in a linear fashion as was reported earlier by Chambonnet *et al.*¹⁹, and assume this reduced expansion is due to the clustering of O-vacancies. Other authors find multiple non-linear regions in the expansion of the lattice parameter. Ryan *et al.*²⁰ link this behavior to the presence of two phases with different La concentration. Of

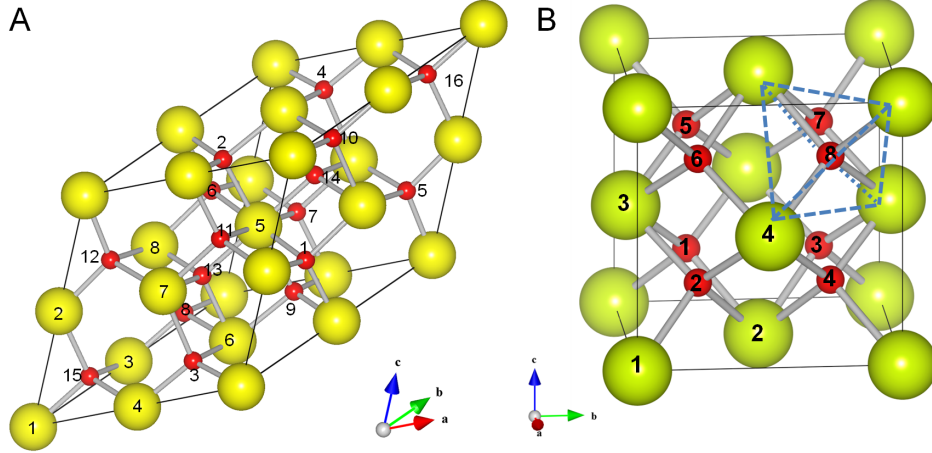


FIG. 1: (Color online) Ball and stick representations of (A) the fcc primitive $2 \times 2 \times 2$ (p222) and (B) the cubic (c111) CeO_2 fluorite super cells. All the inequivalent Ce (big yellow spheres) and O (small red spheres) atom positions are indicated. The dashed tetrahedron on the cubic cell indicates the surrounding tetrahedron around the oxygen atom 8.

these, the phase with the high La density shows a discontinuity in the lattice parameter just around 38% La, and a constant lattice parameter above 40% La. Though they do report observing local ordering in the system, unlike Bae *et al.*⁸, they refrain from linking the second phase to a pyrochlore phase. In contrast, O'Neill and Morris find only a single phase in their investigation of $\text{La}_x\text{Ce}_{1-x}\text{O}_{2-x/2}$.²¹ However, they only go up to a La concentration of 10%, where Ryan *et al.*²⁰ observed the appearance of the second phase at a La concentration of $\sim 20\%$, indicating that below this La concentration, the second phase was either not present or not distinguishable.

As a result of this complex behavior, no definitive crystal structure has been established for $\text{La}_2\text{Ce}_2\text{O}_7$, and there exists only a single entry in the ICSD database, referring back to the work of Zintl and Croatto.^{1,22,23} Experiments are interpreted in favor of the disordered fluorite as well as the pyrochlore structure, and some authors even refer to $\text{La}_2\text{Ce}_2\text{O}_7$ both as a pyrochlore and a fluorite structure in the same work.²⁴

In this paper we present an *ab initio* density functional theory (DFT) study of the $\text{La}_2\text{Ce}_2\text{O}_7$ crystal structure. Based on the order-disorder contrast of the experimentally proposed pyrochlore and disordered fluorite structures, we focus on the effect of order in possible $\text{La}_2\text{Ce}_2\text{O}_7$ structures. By calculating and comparing the formation energies and XRD spectra for a set of different ordered and random structures, we show the pyrochlore structure to be favored over the disordered fluorite structure.

II. THEORETICAL METHOD

Starting from the CeO_2 -fluorite structure, the $\text{La}_2\text{Ce}_2\text{O}_7$ structure is obtained by replacing half of the

TABLE I: O-vacancy and La positions for the different structures investigated. The tetrahedral surrounding of the O-vacancy is indicated as $x\text{Ce}y\text{La}$ with x and y the number of Ce and La atoms in the tetrahedron surrounding the vacancy. The notation NV indicates no vacancies are present in the system. The indexes are shown in Fig. 1A and B. The LZO and L111 structures are generated using the (fluorite) p222 unit cell (*cf.* Fig. 1A).

	La positions	O-vacancies	space group
c111 L1 ₀ NV	1, 2	—	P4/mmm
c111 L1 ₀ 2Ce2La	1, 2	2	Cmm2
LZO NV	5, 6, 7, 8	—	Fd3m
LZO 2Ce2La	5, 6, 7, 8	1, 6	C2/m
LZO 4Ce	5, 6, 7, 8	15, 16	Fd3m
LZO 4La	5, 6, 7, 8	13, 14	Fd3m
L111 NV	1, 6, 7, 8	—	R3m
L111 3Ce1La	1, 6, 7, 8	15, 16	R3m
L111 1Ce3La	1, 6, 7, 8	13, 14	R3m

Ce^{IV} ions by La^{III} (*i.e.* $\text{CeO}_2 \rightarrow \text{La}_2\text{Ce}_2\text{O}_8$), and, due to charge compensation, removing one eighth of the O ions (*i.e.* $\text{La}_2\text{Ce}_2\text{O}_8 \rightarrow \text{La}_2\text{Ce}_2\text{O}_7$). This can be achieved in a large number of ways, resulting in both ordered structures and disordered structures. Because an exhaustive study is impossible within the DFT framework, and because the most prominent difference between the disordered fluorite and pyrochlore structures is their amount of short range order, our study can be confined to some highly ordered structures and a “random structure”. This allows us to investigate the influence of cation-ordering on the stability of the system. Moreover, the chemical environment of the vacancies can be studied in this way.

The three ordered cation distributions we use are: the $\text{La}_2\text{Zr}_2\text{O}_7$ pyrochlore structure (LZO), the cubic CuAu

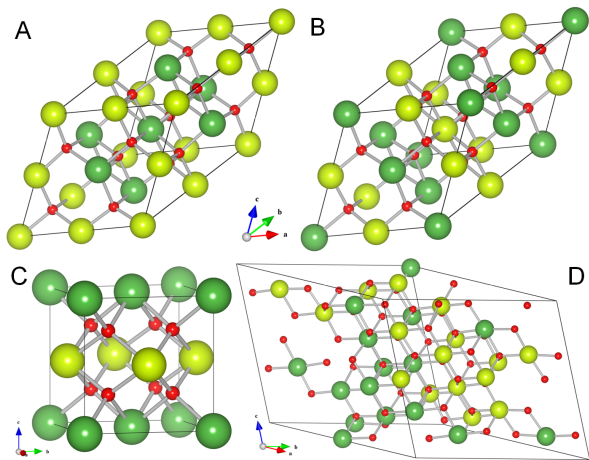


FIG. 2: (Color online) Ball and stick representations of the different cation distributions, as constructed from Table I and Fig. 1 or taken from literature: (A) the LZO, (B) the L111, (C) the c111 $L1_0$ and, (D) the SQS distribution.²⁵ Red, green and yellow spheres show the O, La and Ce positions, respectively.

$L1_0$ structure (c111 $L1_0$), with alternating La and Ce layers along the $[001]$ orientation, and the L111 structure, with alternating Ce and La layers along the $[111]$ orientation. Both the LZO and L111 structures can be constructed using the fluorite p222 primitive fcc supercell, shown in Fig. 1A, the $L1_0$ structure can be constructed using the cubic fluorite supercell, shown in Fig. 1B. For each of these structures a set of O-vacancies is chosen in such a way that all vacancies in a single system have the same chemical environment. Table I gives the positions of the La cations and O-vacancies in the unit cells used for these structures, and shown in Fig. 1A and B, and the resulting cation distributions are shown in Fig. 2A, B, and C. The tetrahedral surrounding (*cf.* Fig. 1B) of the vacancies is indicated as $x\text{Ce}y\text{La}$, with x and y integers giving the number of Ce and La cations in the tetrahedron. Cells without O-vacancies are indicated with NV.

All p222 cells, except the NV structures, contain two vacancies. To improve the comparability of the different structures, the two O-vacancies are always placed symmetrically around a single cation. This way we can assume the contribution to the formation energy due to the O-vacancy interaction energy to be the same for all p222 systems. As a consequence of this setup, all four cations surrounding the O-vacancy in the p222 cells are 6-coordinated. Note that we use the term coordination only to indicate the number of anions present surrounding the cation, not the number of anions the cation has an actual bond with.

There are several methods in literature to obtain physical properties of disordered or random structures. The most intuitive perhaps is the use of averaged potentials in the Virtual Crystal Approximation, where instead of using a specific potential for each ionic species one

uses a potential representing the average atomic species present.²⁶ Another approach is the use of Monte-Carlo methods, and a statistical analysis of the results obtained. However, this method requires one to do thousands (or even more) of calculations, which is not feasible due to the size of our unit cell and the cost of DFT calculations. A third possible approach is the use of cluster expansions, where the configurational dependence of the physical property of interest is described as a sum over bonds or clusters. However, the configurational dependence of any variable can be described exactly by a cluster expansion only if all terms are retained, which is not the case in any practical implementation. Furthermore, predictions of the cluster expansion can depend sensitively on the choices made by the user with regard to for example input structures.^{27,28} We will make use of what is called a Special Quasi-random Structure (SQS).^{29–31} This is a super cell chosen in such a way that the correlation functions of the system resemble those of a truly random system as closely as possible. Although the super cell is a few times larger than a unit cell, and has no symmetry, the fact that we only need to do calculations with a single structure makes this technique orders of magnitude cheaper than a Monte-Carlo method. Neither is it necessary to use statistical methods to obtain system properties.

The main problem with using SQS is the fact that they need to be constructed first. For the pyrochlore(fluorite) system an SQS containing 88(96) atoms was previously given by Jiang *et al.*²⁵. We use this SQS to investigate the physical properties of a disordered fluorite structure. A ball and stick representation is shown in Fig. 2D. Because all possible tetrahedral surroundings for the vacancies are present in this system, no tetrahedral surrounding is indicated.

The electronic structure calculations are performed within the DFT framework using the projector augmented wave (PAW) approach for the core-valence interaction and the Perdew-Burke-Ernzerhof (PBE) approximation for the exchange-correlation functional as implemented in the VASP code.^{32–36} The kinetic energy cut-off is set at 500 eV and special k -point sets of $8 \times 8 \times 8$, $4 \times 4 \times 4$, and $4 \times 4 \times 4$ k -points are used for static self-consistent calculations in the c111, p222 and the SQS cells respectively. For the SQS cells a smaller $2 \times 2 \times 2$ k -point set is used during relaxation. To optimize the geometry a conjugate gradient algorithm is applied. Both ion positions and cell parameters are optimized simultaneously.

Because the $4f$ electron of Ce is known to be badly described in DFT at the PBE-level, we also performed calculations including on-site Coulomb corrections (PBE+U).^{37,38} The inclusion of on-site Coulomb corrections has been shown to provide a consistent treatment of Ce ions in ceria.^{39–43} The choice of U for the Ce $4f$ electrons is found to be optimal in the range of 2–8 eV, depending on which property is under specific investigation.^{41,42,44} For reduced ceria, and a consistent

description of pure CeO_2 and Ce_2O_3 , both Nolan *et al.*³⁹ and Andersson *et al.*⁴¹ suggest for GGA+U a $U_{\text{Ce}} = 5.0$ eV. Because $\text{La}_2\text{Ce}_2\text{O}_7$ contains a large amount of O vacancies, we will follow this suggestion.

In theoretical studies of La doping of ceria surfaces, it was also shown by Yeriskin and Nolan that an on-site Coulomb correction is required to correctly describe the localized hole on the O $2p$ state.⁴⁵ This localized hole results from the introduced La^{III} ion at a Ce^{IV} site. Since the $\text{La}_2\text{Ce}_2\text{O}_7$ structure can be interpreted as an extreme case of La doping we use the same $U_{\text{O}} = 7.0$ eV on the O $2p$ states.

The XRD spectra are generated for the relaxed structures using the visualizer tool of the ICSD database.^{22,23}

III. RESULTS AND DISCUSSION

A. Energetics

The energetics of the system are studied through comparison of the heat of formation ΔH_f and the vacancy formation energies $E_{\text{vac},f}$ of the different configurations. The heat of formation is calculated using:

$$\Delta H_f = (E_{\text{tot}} - N_{\text{Ce}} E_{\text{CeO}_2} - \frac{1}{2} N_{\text{La}} E_{\text{La}_2\text{O}_3} - \frac{1}{2} N_{\text{O}_{\text{add}}} E_{\text{O}_2}) / N_f, \quad (1)$$

with E_{tot} the total ground state energy of the relaxed system, N_{Ce} and N_{La} the number of Ce and La atoms present in the system, E_{CeO_2} and $E_{\text{La}_2\text{O}_3}$ the bulk energy of CeO_2 and La_2O_3 , $N_{\text{O}_{\text{add}}}$ the number of additional O atoms not accounted for by the CeO_2 and La_2O_3 formula units, and E_{O_2} the ground state energy calculated for a free oxygen molecule. The factor N_f is the number of formula units, which we define as the size of a supercell containing a single O-vacancy. The equivalent supercell is used for the systems without vacancies.

The O-vacancy formation energy $E_{\text{vac},f}$ is calculated using:

$$E_{\text{vac},f} = (E_{\text{vac}} + \frac{1}{2} N_{\text{vac}} E_{\text{O}_2} - E_{\text{novac}}) / N_{\text{vac}}, \quad (2)$$

with E_{vac} and E_{novac} the ground state energies obtained for the systems with and without vacancies, respectively, and N_{vac} the total number of vacancies present in the system with O-vacancies. Negative values indicate a stabilization of the system. The resulting energies are shown in Table II.

The calculated heats of formation and O-vacancy formation energies presented in Table II show some clear trends with regard to the stability of $\text{La}_2\text{Ce}_2\text{O}_7$. If no O-vacancies are involved (*i.e.* $\text{La}_2\text{Ce}_2\text{O}_8$) PBE calculations show all possible cation distributions to be roughly degenerate. Including on site Coulomb corrections for Ce and O lifts this degeneracy and shows the disordered fluorite structure to be the most stable. However, $\text{La}_2\text{Ce}_2\text{O}_7$ contains 12.5% O-vacancies compared to the CeO_2 fluo-

rite structure to provide the necessary charge compensation for the introduction of trivalent La in a tetravalent Ce position in the CeO_2 lattice. In contrast to the previous, the introduction of O-vacancies shows no qualitative difference between the PBE and PBE+U results. In both cases the introduction of O-vacancies is beneficial for the heat of formation. The sole exceptions are the systems with three or four La cations in the tetrahedral surrounding of the O-vacancy: L111 1Ce3La (PBE only) and LZO 4La (PBE and PBE+U).

Of all configurations studied, the LZO 4Ce system (*i.e.* the actual pyrochlore structure) has the most favored heat of formation and O-vacancy formation energy. It has a heat of formation that is roughly 0.5 eV/formula unit better than the SQS system, representing the disordered fluorite structure. Closer examination of $E_{\text{vac},f}$ with regard to the tetrahedral surrounding of the O-vacancy shows the following order of increasing stability:

$$4\text{La} < 1\text{Ce}3\text{La} < 2\text{Ce}2\text{La} < 3\text{Ce}1\text{La} < 4\text{Ce}.$$

This shows there is a clear correlation between the number of Ce ions in the surrounding tetrahedron and $E_{\text{vac},f}$. This result is independent of the introduced Coulomb correction, and results for both PBE and PBE+U functionals in an improvement of $E_{\text{vac},f}$ with ~ 1.5 eV, going from the least to the most stable configuration. This also means that ordered structures containing Ce tetrahedra show large stability when the O-vacancies are enclosed in these Ce tetrahedra. On the other hand, structures with no Ce in the tetrahedron surrounding the O-vacancy show poor stability (Compare the LZO 4Ce and LZO 4La structures in Table II. In both cases the cations have a pyrochlore geometry). Due to this stability trend for O-vacancy positions, it is clear why the disordered fluorite structure (*i.e.* SQS) is less favorable than ordered structures. Because of the random nature of the disordered fluorite structure, fewer pure Ce tetrahedra are present. In addition, because of their random distribution, the O-vacancies are also placed in less favorable surroundings than could be the case in ordered structures.

Irrespective of the correlation between $E_{\text{vac},f}$ and the number of Ce cations in the tetrahedral O-vacancy surrounding, there still appears to be quite some variation in formation energies for the same surrounding when comparing the two 2Ce2La structures in Table II. These two systems differ in two aspects: the inter-vacancy distance and the coordination of the cations in the system. This leads to the question which of both is responsible for the difference in vacancy formation energy.

We have studied two sets of additional systems, given in Table III, to further investigate the influence of these aspects. The first set consists of the p222 L1₀ structure. This is the L1₀ distribution of the cations but this time constructed using a p222 unit cell (*cf.* Fig. 1 and Table III). The O-vacancies are placed at opposing sides of a single Ce cation,⁴⁶ reducing the

TABLE II: The heat of formation ΔH_f and vacancy formation energy $E_{vac,f}$ as calculated using equations (1) and (2). The inter-vacancy distance $d_{vac-vac}$ is calculated as the distance between the centers of mass of the cation tetrahedra surrounding the O-vacancies. Due to the random nature of the SQS system no inter-vacancy distance is given. The notation NV is used to identify systems without vacancies. For the PBE+U calculations we use $U_O = 7.0$ eV on the O 2p states and $U_{Ce} = 5.0$ eV on the Ce 4f states for all calculations involved.

	PBE			PBE+U		
	ΔH_f (eV)	$E_{vac,f}$ (eV)	$d_{vac-vac}$ (Å)	ΔH_f (eV)	$E_{vac,f}$ (eV)	$d_{vac-vac}$ (Å)
c111 L1 ₀ NV	1.177	—	—	1.280	—	—
c111 L1 ₀ 2Ce2La	0.758	-0.419	5.576	0.800	-0.480	5.570
LZO NV	1.167	—	—	1.364	—	—
LZO 2Ce2La	0.939	-0.229	4.829	1.105	-0.259	4.818
LZO 4Ce	-0.016	-1.183	4.861	0.220	-1.143	4.862
LZO 4La	1.668	0.501	4.812	1.620	0.256	4.803
L111 NV	1.169	—	—	1.564	—	—
L111 3Ce1La	0.452	-0.717	4.782	0.668	-0.896	4.787
L111 1Ce3La	1.352	0.183	4.843	1.420	-0.144	4.843
SQS NV	1.160	—	—	0.699	—	—
SQS	0.527	-0.633	n/a	0.607	-0.91	n/a

TABLE III: O-vacancy and La positions for some additional structures. The ‘L111 3Ce1La’ structure of Table I has been repeated here as ‘L111 3Ce1La A’ for comparison.

	La positions	O-vacancies	space group
p222 L1 ₀ NV	1, 2, 5, 6	—	P4/mmm
p222 L1 ₀ 2Ce2La	1, 2, 5, 6	1, 6	Imma
L111 3Ce1La A	1, 6, 7, 8	15, 16	R3m
L111 3Ce1La B	1, 6, 7, 8	1, 7	Pm
L111 3Ce1La C	1, 6, 7, 8	7, 9	C2/m

inter-vacancy distance by about 0.8 Å compared to the c111 L1₀ structure. At the same time, the coordination changes from 7-fold coordination for all cations in the c111 L1₀ structure to 6-fold coordination for half the Ce and half the La ions and 8-fold coordination for the remaining cations in the p222 L1₀ structure. A second set of structures consists of L111 3Ce1La B and C (*cf.* Table III), where the former L111 3Ce1La structure will be referred to as L111 3Ce1La A. Table IV gives the energies, inter-vacancy distances and Ce-coordination for these systems.

Comparing L1₀ structures in Tables II and IV shows that the heat of formation, ΔH_f , is exactly the same, as it should be, when no vacancies are present. However, with O-vacancies included, there is a significant difference in $E_{vac,f}$ of 0.2 – 0.3 eV. This difference between the c111 and p222 L1₀ 2Ce2La systems is related to their different vacancy configurations. Comparing the three 2Ce2La systems studied, we find that both systems with half the Ce ions 6-fold coordinate are ~ 0.2 eV less stable than the third system (c111 L1₀ 2Ce2La), without 6-fold coordinate Ce.

The three L111 3Ce1La configurations can also be used to distinguish the effects of distance and coordination. Due to the three different inter-vacancy

distances and the same Ce coordination for the B and C structures one can consider following scenarios: If a large O-vacancy distance is beneficial to the system then the O formation energies should be ranked $A < B < C$, with A the best configuration. Contrary, if the opposite is the case, namely clustering or coalescing of the vacancies is beneficial, the C case should be the best structure, giving rise to a ranking $C < B < A$. In both these scenarios the Ce coordination is assumed to have little or no influence. If on the other hand the inter-vacancy distance has little or no influence and the reduced number of 6-fold coordinate Ce cations causes the decreased vacancy formation energy, then the B and C case should be (nearly) degenerate and more stable than the A case. The resulting ranking should then be $A > B = C$.

Comparing the energies in Table II and IV we see a significant improvement (~ 0.4 eV) in the heat of formation and O-vacancy formation energy for the B and C configurations compared to A. This change is comparable to the one found for the L1₀ 2Ce2La structures. Table IV also shows the B and C configurations to be roughly degenerate. This shows that the improved energetics originate from the third scenario described above. The reduced number of 6-fold coordinate Ce ions causes a significant improvement of the formation energy $E_{vac,f}$. Upon closer examination we also notice that the B configuration is slightly more stable (~ 0.06 eV) than the C configuration, showing that also the O-vacancy distance plays a role, albeit a minor one, and, more importantly, that the vacancies repel each other.

The results of this section also give us some additional understanding on the structure of $La_x Ce_{1-x} O_{2-x/2}$. The above calculations show that for $La_2 Ce_2 O_7$ the Ce atoms prefer to cluster in tetrahedra around the O-vacancies, or vice versa, the O-vacancies prefer to appear inside Ce tetrahedra. If we assume that this behavior is also valid

TABLE IV: The same as Table II, for the additional structures. In addition, also the distribution of the Ce coordination is given. The c111 L1₀ 2Ce2La and L111 3Ce1La A structures are repeated from Table II for comparison.

	Ce-Coord. (6 7 8)-fold (%)	PBE			PBE+U		
		ΔH_f (eV)	$E_{vac,f}$ (eV)	$d_{vac-vac}$ (Å)	ΔH_f (eV)	$E_{vac,f}$ (eV)	$d_{vac-vac}$ (Å)
p222 L1 ₀ NV	(0 0 100)	1.178	—	—	1.281	—	—
p222 L1 ₀ 2Ce2La	(50 0 50)	1.007	-0.171	4.784	1.115	-0.166	4.776
c111 L1 ₀ 2Ce2La	(0 100 0)	0.758	-0.419	5.576	0.800	-0.480	5.570
L111 3Ce1La A	(75 0 25)	0.452	-0.717	4.782	0.668	-0.896	4.787
L111 3Ce1La B	(50 50 0)	0.072	-1.097	3.960	0.198	-1.366	3.945
L111 3Ce1La C	(50 50 0)	0.123	-1.046	2.937	0.263	-1.301	2.934

TABLE V: Geometric data for the PBE and PBE+U results. We use the notation NV to indicate systems without vacancies. For these NV systems ΔV is calculated with regard to the volume of the equivalent CeO₂ fluorite cell, while for the other systems it is calculated with regard to the NV system. The lattice parameter a (see text) is calculated as $a = \sqrt[3]{V_f}$, and Δa gives the change of this lattice parameter with regard to the lattice parameter of CeO₂ fluorite and the calculated lattice parameter of the NV system.

	PBE				PBE+U			
	ΔV	a	Δa		ΔV	a	Δa	
	(%)	(Å)	vs CeO ₂ (%)	vs NV (%)	(%)	(Å)	vs CeO ₂ (%)	vs NV (%)
c111 L1 ₀ NV	8.044	5.606	2.613	—	7.945	5.609	2.581	—
c111 L1 ₀ 2Ce2La	-1.260	5.582	2.180	-0.422	-1.631	5.579	2.021	-0.547
p222 L1 ₀ NV	8.080	5.606	2.624	—	7.947	5.609	2.582	—
p222 L1 ₀ 2Ce2La	-1.281	5.582	2.184	-0.429	-1.725	5.577	1.989	-0.578
LZO NV	8.328	5.611	2.702	—	8.479	5.618	2.750	—
LZO 2Ce2La	-0.668	5.598	2.473	-0.223	-1.533	5.590	2.222	-0.514
LZO 4Ce	0.108	5.613	2.739	0.036	-0.228	5.614	2.672	-0.076
LZO 4La	-2.889	5.556	1.704	-0.973	-3.793	5.547	1.434	-1.281
L111 NV	8.253	5.609	2.679	—	8.639	5.621	2.800	—
L111 3Ce1La A	-0.292	5.604	2.579	-0.097	-1.045	5.602	2.441	-0.350
L111 3Ce1La B	-0.081	5.608	2.651	-0.027	-0.889	5.605	2.495	-0.297
L111 3Ce1La C	0.299	5.615	2.781	0.099	-0.459	5.613	2.643	-0.153
L111 1Ce3La	-1.736	5.577	2.081	-0.582	-2.774	5.569	1.841	-0.933
SQS NV	8.530	5.614	2.766	—	9.173	5.630	2.969	—
SQS	-0.020	5.614	2.759	-0.007	-1.285	5.606	2.526	-0.430

for La_xCe_{1-x}O_{2-x/2}, then the transformation of CeO₂ to La₂Ce₂O₇ can be understood as follows: For low La concentrations, and thus low O-vacancy concentrations, the vacancies, imbedded in Ce tetrahedra, will be distributed homogeneously throughout the CeO₂ fluorite structure. With increasing La concentration the number of available Ce cations for Ce tetrahedra reduces while the number of O-vacancies increases. For a system where the cations are randomly distributed this means that at La concentrations of > 42.8% there are too few Ce-tetrahedra available to accommodate all the O-vacancies. This seems to coincide with the experimentally observed discontinuity in the lattice parameter observed by Bae *et al.*⁸ As a result, the attraction between Ce cations and O-vacancies can thus be seen as the driving force for order in the La₂Ce₂O₇ system. Such a link between the ordering of the cation and anion sub-lattices is also found for other pyrochlores.⁴⁷ The resulting geometry at 50% Ce substituted by La, is then expected to be a highly ordered

structure containing Ce tetrahedra surrounding the O-vacancies. This makes the pyrochlore geometry a very likely candidate for the La₂Ce₂O₇ geometry.

B. Lattice parameter

In addition to the energies, we also investigated the cell volume and lattice parameter. Table V shows the expansion and contraction of the system compared to the pure CeO₂ fluorite structure. Most configurations studied show small distortions of the lattice vectors compared to the cubic fluorite lattice. Only the LZO NV, 4Ce, and 4La configurations retained a cubic lattice.

Because the distortions of the different system lattices are all slightly different, it is impossible to extract a (consistent) lattice parameter from their basis vectors. However, since the distortions are relatively small, less than 4° for the lattice vector angles, and less than 3.5%

for the lattice vector lengths, we instead choose to use a fictitious lattice parameter, which is determined as the edge of a cube containing a single formula unit, with the same mass density as the actual crystal.

Comparing the results in Table V shows the Coulomb corrections to have only limited influence on the geometry. Compared to the CeO_2 fluorite system, the $\text{La}_2\text{Ce}_2\text{O}_7$ systems without vacancies are roughly 8% larger in volume. The introduction of O-vacancies causes a small contraction of the lattice parameter of a few tenth of a percent compared to the NV systems. This contraction appears to be correlated to the amount of Ce atoms present in the tetrahedral vacancy surrounding; more Ce results in less contraction. This behavior can be understood as a consequence of the increase in ionic radius known for the $\text{Ce}^{\text{IV}} \rightarrow \text{Ce}^{\text{III}}$ transition.^{48,49}

It is also interesting to note that for the L111 3Ce1La cases the lattice parameter seems to increase with decreasing O-vacancy distance, in contrast to what is intuitively expected.

Looking at the three most stable configurations with regard to $E_{\text{vac},f}$ of the previous section (LZO 4Ce, L111 3Ce1La B and C), we find that these are also the three systems having the largest lattice parameter. Their lattice parameter is 5.61 Å, which is $\sim 2.6\%$ larger than the normal CeO_2 fluorite structure. This is in good agreement with the experimentally observed value of 5.53 – 5.61 Å for the $\text{La}_2\text{Ce}_2\text{O}_7$ lattice parameter.^{8,9,15,50,51} It also shows good agreement with the experimentally observed relative expansion of $\sim 2.8\%$ by Ryan *et al.* and Bellière *et al.*^{20,50} In addition, the pyrochlore structure LZO 4Ce is the only one of these three structures which retained a perfect cubic lattice, as expected from experiment for $\text{La}_2\text{Ce}_2\text{O}_7$.¹⁵

C. X-Ray diffraction

An important argument in the discussion on the structure of $\text{La}_2\text{Ce}_2\text{O}_7$ is its XRD spectrum. The differences between the CeO_2 fluorite and a prototypical pyrochlore spectrum are very small and mainly related to the presence of the low intensity peaks of the pyrochlore (311), (331), and (511) reflections.^{8,9,53} The strong similarity between the CeO_2 and pyrochlore spectra is due to the nearly equal X-ray scattering factors of La and Ce.¹⁵ As a result very sensitive XRD experiments are required if one is to observe the low intensity peaks indicative of the pyrochlore structure of $\text{La}_2\text{Ce}_2\text{O}_7$.

To address this point in the discussion, we calculated XRD spectra for all structures studied. Figure 3 shows calculated spectra of the SQS (disordered fluorite) and LZO 4Ce (pyrochlore) geometries in comparison to an experimental powder XRD spectrum of $\text{La}_2\text{Ce}_2\text{O}_7$.⁵² The experimental spectrum shows nine clear peaks that can be identified with the fluorite peaks of CeO_2 , no small secondary pyrochlore peaks are visible. This is

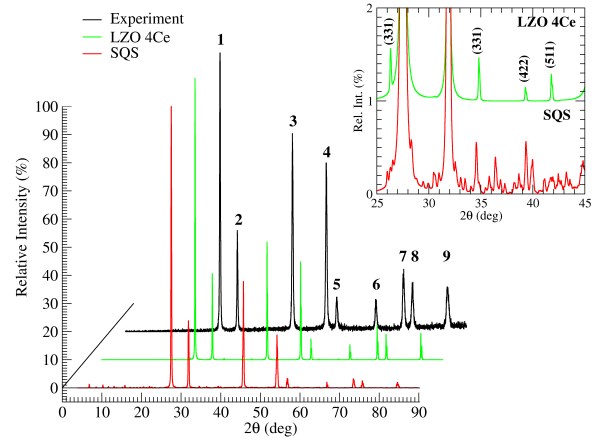


FIG. 3: (Color online) Comparison of calculated XRD images for the disordered fluorite (SQS, red curve at the front) and pyrochlore (LZO 4Ce, green curve in the middle) geometries to the experimental $\text{La}_2\text{Ce}_2\text{O}_7$ spectrum (black curve at the back).⁵² The relaxed PBE geometries are used to calculate the XRD spectra. The nine peaks with the highest intensity are indicated with indexes 1 through 9. All spectra are normalized with regard to the peaks with index 1. The inset shows a section of the spectra containing the pyrochlore (311), (331), and (511) peaks. The LZO 4Ce curve was shifted vertically by 1% for clarity.

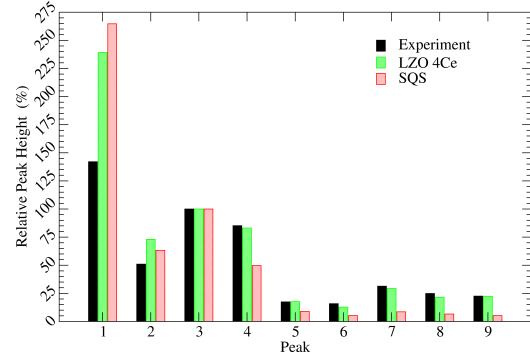


FIG. 4: (Color online) Comparison of the nine high intensity peaks present in the spectra shown in Fig. 3. Scaling was done with regard to the third peak for each spectrum.

in line with the XRD spectra of $\text{La}_2\text{Ce}_2\text{O}_7$ generally presented in literature. The two calculated spectra in Fig. 3 represent the spectra of the two possible structures for the $\text{La}_2\text{Ce}_2\text{O}_7$ structure. In both calculated spectra the nine experimental peaks are clearly visible and their position is still within 1° of the experimental position for the high angle peaks. Furthermore, no additional peaks with intensities $> 1\%$ are visible in the calculated spectra.

It is interesting to note that even if a pyrochlore geometry is used, the typical pyrochlore peaks appear

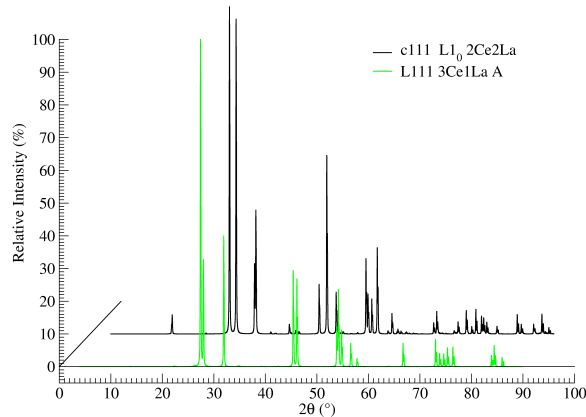


FIG. 5: (Color online) Calculated XRD-spectra of the c111 L1₀ 2Ce₂La and L111 3Ce₁La A structures. Multiple peak splitting is clearly visible for the high angle peaks.

to be lacking. However, closer examination of the numerical data shows these peaks to be present, albeit at a much lower intensity than would be expected from other pyrochlore systems such as for example La₂Zr₂O₇. The (311), (331) and (511) peaks have an intensity of 0.5% or less (*cf.* inset Fig. 3). This explains why these peaks are not generally observed in experiments, but only in case of long time step scans.⁸ This might lead to an erroneous assignment of the disordered fluorite structure to La₂Ce₂O₇. The SQS structure on the other hand presents a large number of very small secondary reflections. Though they might not be clearly distinguishable in experiments, they should introduce a noticeable additional background (*cf.* inset Fig. 3). This should be especially clear in experiments where increasing La concentrations in La_xCe_{1-x}O_{2-x/2} are investigated. However, such experiments do not mention such behavior.^{8,20}

A thorough comparison of the nine high intensity peaks also favors the pyrochlore (LZO 4Ce) over the disordered fluorite (SQS) structure, as geometry for La₂Ce₂O₇. The relative peak heights of the former match the experimental peak heights much closer, as is shown in Fig. 4. We chose not to scale the spectra using the highest intensity peak since it appears to be overestimated for both geometries. By using a different peak as scaling reference the good correlation of the relative peak heights, with the experimental spectrum becomes much clearer.

As a final note, it is interesting to mention that the four high angle peaks, can also be used to exclude the other structures studied in this work. This is because of the broadening of those peaks due to multiple splitting. As a consequence, the two peaks between 70 and 80° merge into a near continuous set of peaks spread over a range of 5° in case of the L111 structures, and nearly 10° in case of the L1₀ structures. Two examples are given in Fig. 5. No simple peaks, as present in the curves of

Fig. 3 are observed for those structures.

IV. CONCLUSION

In this paper the geometry of La₂Ce₂O₇ was studied using *ab initio* DFT calculations. Ordered and disordered structures were compared, modeling the pyrochlore and the disordered fluorite structures proposed for this system. Three aspects are taken into consideration: the lattice parameter, the enthalpy of formation and the XRD spectrum.

The calculated lattice parameters and relative lattice expansion of both the pyrochlore and disordered fluorite geometry are found to be in good agreement with the experimentally observed values. Of these the pyrochlore structure retained a perfect cubic lattice, while the disordered fluorite structure showed a small distortion.

Charge compensating O-vacancies are shown to play a crucial role in the stability of La₂Ce₂O₇. If no O-vacancies are present (*i.e.* La₂Ce₂O₈) the disordered fluorite structure is the most stable geometry. However, if O-vacancies are included in the system, then the pyrochlore structure becomes the most stable geometry. So, in contrast to what is generally assumed in literature, La₂Ce₂O₇ is predicted to have a pyrochlore rather than a disordered fluorite geometry.

Total energy calculations have also shown a clear preference of the O-vacancies to be centered in Ce tetrahedra. This might be seen as a driving force in the formation of a pyrochlore geometry during La₂Ce₂O₇ formation. The formation of La₂Ce₂O₇, however, is beyond the scope of this work, and is, as such, a topic for further research.

The third aspect, the XRD spectra, show for both the disordered fluorite and pyrochlore geometry the nine distinct high intensity peaks observed for La₂Ce₂O₇ in experiment. Although the peak positions are in excellent agreement with the experimental positions, only the pyrochlore geometry presents relative peak intensities that are in good agreement with the experimental ones. Furthermore, the pyrochlore geometry also presents the typical pyrochlore reflection peaks, albeit with a lower intensity than expected from other pyrochlores.

Finally, both formation energies and calculated XRD spectra show a highly ordered structure to be preferred over a disordered structure, as model for the La₂Ce₂O₇ system. Of the structures considered in this work, the pyrochlore geometry is clearly favorable over the disordered fluorite geometry.

V. ACKNOWLEDGEMENT

We would like to thank Olivier Janssens and Vyshnavi Narayanan for the XRD measurements. The research

was financially supported by FWO-Vlaanderen, project n° G. 0802.09N. We also acknowledge the Research Board of the Ghent University. All calculations were carried out using the Stevin Supercomputer Infrastructure at Ghent

University. XRD measurements were carried out under the Interuniversity Attraction Poles Programme IAP/VI-17 (INANOMAT) financed by the Belgian State, Federal Science Policy office.

- ¹ E. Zintl and U. Croatto, *Z. Anorg. Allg. Chem.* **242**, 79 (1939).
- ² F. Deganello and A. Martorana, *J. Solid State Chem.* **163**, 527 (2002).
- ³ F. Deganello, A. Longo, and A. Martorana, *J. Solid State Chem.* **175**, 289 (2003), ISSN 0022-4596.
- ⁴ M. Reddy, Benjaram, L. Katta, and G. Thrimurthulu, *Chem. Mater.* **22**, 467 (2010).
- ⁵ S. Liang, E. Broitman, Y. Wang, A. Cao, and G. Vesper, *J. Mater. Sci.* **46**, 2928 (2011).
- ⁶ H. L. Tuller and A. S. Nowick, *J. Electrochem. Soc.* **122**, 255 (1975).
- ⁷ T. Kudo and H. Obayashi, *J. Electrochem. Soc.* **122**, 142 (1975).
- ⁸ J. S. Bae, W. K. Choo, and C. H. Lee, *J. Eur. Ceram. Soc.* **24**, 1291 (2004).
- ⁹ X. Cao, R. Vassen, W. Fischer, F. Tietz, W. Jungen, and D. Stover, *Adv. Mater.* **15**, 1438 (2003).
- ¹⁰ W. Ma, S. Gong, H. Xu, and X. Cao, *Scripta Mater.* **54**, 1505 (2006).
- ¹¹ X. Q. Cao, R. Vassen, and D. Stoeber, *J. Eur. Ceram. Soc.* **24**, 1 (2004).
- ¹² I. Van Driessche, G. Penneman, E. Bruneel, and S. Hoste, *Pure Appl. Chem.* **74**, 2101 (2002).
- ¹³ I. Van Driessche, G. Penneman, J. S. Abell, E. Bruneel, and S. Hoste, *Thermec'2003*, parts 1–5 **426-4**, 3517 (2003).
- ¹⁴ I. Van Driessche, G. Penneman, C. De Meyer, I. Stambolova, E. Bruneel, and S. Hoste, in *Euro Ceramics VII, PT 1-3* (2002), vol. 206-2 of *Key Engineering Materials*, pp. 479–482.
- ¹⁵ F. Brisse and O. Knop, *Can. J. Chem.* **45**, 609 (1967).
- ¹⁶ L. Minervini, R. W. Grimes, and K. E. Sickafus, *J. Am. Ceram. Soc.* **83**, 1873 (2000).
- ¹⁷ H. Yamamura, H. Nishino, K. Kakinuma, and K. Nomura, *J. Ceram. Soc. Jpn* **111**, 902 (2003).
- ¹⁸ H. Yamamura, H. Nishino, and K. Kakinuma, *J. Ceram. Soc. Jpn* **112**, 553 (2004).
- ¹⁹ D. Chambonnet, D. Keller, and C. Belouet, *Physica C* **302**, 198 (1998).
- ²⁰ K. M. Ryan, J. P. McGrath, R. A. Farrell, W. M. O'Neill, C. J. Barnes, and M. A. Morris, *J. Phys. Condens. Matter* **15**, L49 (2003).
- ²¹ W. M. O'Neill and M. A. Morris, *Chem. Phys. Lett.* **305**, 389 (1999).
- ²² G. Bergerhoff and I. D. Brown, in *Crystallographic Databases*, edited by F. H. Allen, G. Bergerhoff, and R. Sievers (International Union of Crystallography, Chester, 1987), vol. 77.
- ²³ A. Belsky, M. Hellenbrandt, V. L. Karen, and Luksch, *Acta Cryst. B* **58**, 364 (2002).
- ²⁴ F. W. Bezerra Lopes, C. P. de Souza, A. M. Vieira de Moraes, J.-P. Dallas, and J.-R. Gavarrí, *Hydrometallurgy* **97**, 167 (2009).
- ²⁵ C. Jiang, C. R. Stanek, K. E. Sickafus, and B. P. Uberuaga, *Phys. Rev. B* **79**, 104203 (2009).
- ²⁶ N. J. Ramer and A. M. Rappe, *Phys. Rev. B* **62**, R743 (2000).
- ²⁷ D. Lerch, O. Wieckhorst, G. L. W. Hart, R. W. Forcade, and S. Mueller, *Modell. Simul. Mater. Sci. Eng.* **17** (2009).
- ²⁸ J. Sanchez, F. Ducastelle, and D. Gratias, *Physica A* **128**, 334 (1984).
- ²⁹ A. Zunger, S.-H. Wei, L. G. Ferreira, and J. E. Bernard, *Phys. Rev. Lett.* **65**, 353 (1990).
- ³⁰ S.-H. Wei, L. G. Ferreira, J. E. Bernard, and A. Zunger, *Phys. Rev. B* **42**, 9622 (1990).
- ³¹ A. V. Ruban, S. I. Simak, S. Shallcross, and H. L. Skriver, *Phys. Rev. B* **67**, 214302 (2003).
- ³² P. E. Blöchl, *Phys. Rev. B* **50**, 17953 (1994).
- ³³ G. Kresse and D. Joubert, *Phys. Rev. B* **59**, 1758 (1999).
- ³⁴ G. Kresse and J. Hafner, *Phys. Rev. B* **47**, 558 (1993).
- ³⁵ G. Kresse and J. Furthmüller, *Phys. Rev. B* **54**, 11169 (1996).
- ³⁶ J. P. Perdew, K. Burke, and M. Ernzerhof, *Phys. Rev. Lett.* **77**, 3865 (1996).
- ³⁷ A. Svane, *Phys. Rev. B* **53**, 4275 (1996).
- ³⁸ N. V. Skorodumova, R. Ahuja, S. I. Simak, I. A. Abrikosov, B. Johansson, and B. I. Lundqvist, *Phys. Rev. B* **64**, 115108 (2001).
- ³⁹ M. Nolan, S. Grigoleit, D. C. Sayle, S. C. Parker, and G. W. Watson, *Surface Science* **576**, 217 (2005).
- ⁴⁰ S. Fabris, S. de Gironcoli, S. Baroni, G. Vicario, and G. Balducci, *Phys. Rev. B* **71**, 041102 (2005).
- ⁴¹ D. A. Andersson, S. I. Simak, B. Johansson, I. A. Abrikosov, and N. V. Skorodumova, *Phys. Rev. B* **75**, 035109 (2007).
- ⁴² C. Loschen, J. Carrasco, K. M. Neyman, and F. Illas, *Phys. Rev. B* **75**, 035115 (2007).
- ⁴³ J. L. F. Da Silva, *Phys. Rev. B* **76**, 193108 (2007).
- ⁴⁴ C. W. M. Castleton, J. Kullgren, and K. Hermansson, *J. Chem. Phys.* **127**, 244704 (pages 11) (2007).
- ⁴⁵ I. Yeriskin and M. Nolan, *J. Phys.: Condens. Matter* **22**, 135004 (2010).
- ⁴⁶ The two O-vacancies, at positions 1 and 6 of the p222 cell shown in Fig. 1A, are located, due to periodic boundary conditions, at opposing sides of the La site 2, the Ce site 3, the La site 5, and the Ce site 8. This causes half the Ce cations of the system to have two neighboring O-vacancies, and half the Ce cations to have no neighboring O-vacancies. In contrast, every Ce cation in the c111 L1₀ system (*cf.* Fig. 1B) has exactly one neighboring O-vacancy.
- ⁴⁷ J.-P. Crocombette and A. Chartier, *Nucl. Instrum. Methods Phys. Res., Sect. B* **255**, 158 (2007).
- ⁴⁸ R. D. Shannon, *Acta Cryst.* **A32**, 751 (1976).
- ⁴⁹ J. D. Van Horn, *Electronic Table of Shannon Ionic Radii* (2001), downloaded 08/13/2010, URL <http://v.web.umkc.edu/vanhornj/shannonradii.htm>.
- ⁵⁰ V. Bellière, G. Joorst, O. Stephan, F. M. F. de Groot, and B. M. Weckhuysen, *J. Phys. Chem. B* **110**, 9984 (2006).
- ⁵¹ B. C. Morris, W. R. Flavell, W. C. Mackrodt, and M. A.

- Morris, J. Mater. Chem. **3**, 1007 (1993).
- ⁵² V. Narayanan, D. E. P. Vanpoucke, P. Lommens, E. Bruneel, K. De Buysser, and I. Van Driessche, to be submitted (2011).
- ⁵³ H. Yamamura, H. Nishino, K. Kakinuma, and K. Nomura, Solid State Ionics **178**, 233 (2007).